Linear and nonlinear current response in disordered *d*-wave superconductors

L. Benfatto,[1] C. Castellani,[1] and G. Seibold[2]
[1]*Dipartimento di Fisica, Università di Roma "La Sapienza", and ISC-CNR, Piazzale Aldo Moro 5, 00185 Roma, Italy*
[2]*Institut für Physik, BTU Cottbus-Senftenberg, D-03013 Cottbus, Germany*

(Received 24 July 2023; revised 6 October 2023; accepted 6 October 2023; published 20 October 2023)

We present a detailed theoretical investigation of the linear and nonlinear optical response in a model system for a disordered *d*-wave superconductor. By evaluating the quasiparticle contribution (BCS response) we show that for both quantities the gap symmetry considerably changes the paradigm of the optical response as compared to the conventional *s*-wave case. For what concerns the linear response our findings agree with previous work showing that in strongly disordered *d*-wave superconductors a large fraction of uncondensed spectral weight survives below T_c, making the optical absorption around the gap-frequency scale almost unchanged with respect to the normal state. Our numerical results are in excellent quantitative agreement with experiments in overdoped cuprates. In the nonlinear regime we focus on the third-harmonic generation (THG), finding that, as already established for the *s*-wave case, in general a large THG is triggered by disorder-activated paramagnetic processes. However, in the *d*-wave case the BCS response is monotonously increasing in frequency, losing any signature of THG enhancement when the THz pump frequency ω matches the gap maximum Δ, a hallmark of previous experiments in conventional *s*-wave superconductors. Our findings, along with the mild polarization dependence of the response, provide an explanation for recent THG measurements in cuprates, setting the framework for the theoretical understanding of nonlinear effects in unconventional cuprates.

DOI: 10.1103/PhysRevB.108.134508

I. INTRODUCTION

Since the discovery of high-critical temperature (T_c) superconductivity in cuprates, optical-conductivity measurements have been central in advancing our understanding of their unusual electronic properties, including, e.g., the symmetry of the superconducting (SC) gap, the opening of a pseudogap above T_c, or the transition from a Mott-insulating state to a (non-) Fermi liquid with increasing doping (for a review see, e.g., Refs. [1,2]). In more recent years, the development of nonequilibrium spectroscopies, made possible by the use of intense light pulses, offered the potential opportunity to disentangle different dynamical processes at play in complex systems via their different relaxation times [3]. With regard to SC materials, the advent of THz spectroscopy at strong fields turned out to be particularly promising, due to the frequency-matching condition between the light and the typical energy scales at play in the SC phenomenon. This condition allows one to observe relevant effects already with pump-only experiments, thanks to the ability of the intense light pulses to trigger via nonlinear optical processes collective excitations invisible in the linear response. This is the case, e.g., for the long-sought amplitude or Higgs mode of the superconductor, that couples to light only to quadratic order, being charge neutral [4].

A paradigmatic demonstration of nonlinear THz processes is provided by the measurement of enhanced third-harmonic generation (THG) below T_c that has been demonstrated so far in a variety of systems, ranging from conventional NbN [5–7] and MgB_2 [8,9] superconductors and more recently in unconventional pnictides [10] and cuprate superconductors [11–16]. From the theoretical point of view, the interpretation of these experiments can still rely on a quasiequilibrium scheme, provided that the optical response is computed beyond linear order. Basically, the current density in response to an applied vector potential $\mathbf{A}(t)$ can be expanded up to third order as

$$j_\alpha = \chi^{(1)}_{\alpha\beta} A_\beta + \chi^{(3)}_{\alpha\beta\gamma\delta} A_\beta A_\gamma A_\delta, \tag{1}$$

where $\chi^{(1)}$ is the linear response which is related to the optical conductivity and $\chi^{(3)}$ is the nonlinear optical kernel. Despite such a considerable simplification with respect to the pure nonequilibrium phenomena, the interpretation of the THG experiments on superconductors stimulated so far considerable theoretical work [17–28]. The reason is that in an *s*-wave superconductor both the direct contribution to $\chi^{(3)}$ of BCS quasiparticles and of the amplitude fluctuations of the order parameter give the largest response to THG when the frequency ω of the THz pump matches the value of the SC gap, $\omega = \Delta$, making it difficult to disentangle the two effects in the experimental results. In the case of *s*-wave superconductors it has been so far established that the hierarchy among the two contributions is ruled in a crucial way by disorder effects. Indeed, while for clean single-band [19] and multiband [20] *s*-wave superconductors the THG is dominated by diamagneticlike processes, yielding a predominant response from BCS quasiparticles, disorder makes possible also paramagneticlike processes which also couple nonlinearly the light to the system [21–23,25]. The consequences are twofold: From one side, the strength of the THG is overall enhanced even by weak disorder while still retaining a rather sharp resonance at $\omega = \Delta$, explaining thus the rather large effects measured in the experiments. From the other side, at relatively strong disorder the Higgs response can eventually overcome the BCS

one, allowing for a preferential channel to drive the Higgs mode by light. In addition, disorder influences also the polarization dependence of the THG signal, i.e., the dependence of the generated nonlinear current on the angle that the applied field **A** forms with the main crystallographic axes of the lattice. So far, numerical studies [25,28] accounting exactly for disorder effects on a prototypical square lattice showed that the THG response, that is strongly polarization dependent in the clean limit [19], becomes rather isotropic already at moderate disorder, in agreement with usual observations in both s-wave [6,7] and d-wave [11,14,15] superconductors.

For d-wave superconductors theoretical studies of THG have been restricted until now to the clean limit [24], confirming the predominance of the BCS response in this regime. In addition, these studies find that even though in a d-wave superconductor a continuum of BCS excitations exists below twice the gap maximum Δ even at $T = 0$, the nonlinear kernel $\chi^{(3)}$ preserves in the clean limit a strong resonance at 2Δ and a pronounced polarization dependence. However, both effects seem to be in contrast with the experimental observations in cuprates [11,14–16], where the THG has been investigated as a function of temperature at fixed pump frequency. Varying the temperature changes the order parameter $\Delta(T)$ and thus the optical gap $2\Delta(T)$. Unexpectedly, the THG signal has a rather smooth temperature dependence, with no clear signatures of a resonance effect at the temperature where the pumping frequency matches the maximum gap value and it has a mild polarization dependence. In addition, the THG is found to persist on a wide range of temperatures above T_c, calling for the possible contribution of fluctuation effects due to the THz probing frequency [29].

In this manuscript we address explicitly the role of disorder on the THG response of a d-wave superconductor. In general, cuprates are usually expected to be in the relatively clean limit, at least for underdoped and optimally doped samples, where optical-conductivity measurements in the THz regime [30] suggest a value $1/(2\Delta\tau) \simeq 0.85$, with τ being the transport scattering rate. Nonetheless, already such a small disorder can significantly enhance the THG response and affect the polarization dependence, as it has been shown [28] in some recent work with the band dispersion of cuprates and s-wave order-parameter symmetry.

The situation can be eventually different for strongly overdoped cuprates, as, e.g., in overdoped LSCO films [31,32], where already the linear optical response revealed a significant uncondensed fraction of charge carriers and a concomitant "Drude"-like behavior of $\sigma_1(\omega)$ even below T_c. These data, together with the experimentally found correlation between T_c and the superfluid density [33] in the overdoped regime, have stimulated the idea that disorder, presumably due to out-of plane dopant ions, is a key player in understanding the vanishing of T_c in this doping range [34–36].

To address these issues we compute the linear and nonlinear current response within a disordered lattice model where the d-wave SC order is induced via a Heisenberg-like spin-spin interaction. As compared to previous work in the s-wave case [25,28], the challenge here is the necessity to carry out the numerical simulations with large lattices, since the low-energy response is dominated by the nodal regions where the SC gap vanishes. This is indeed the origin [37] of the so-called universal value σ_0 of the optical conductivity in the limit $\omega \to 0$, i.e., a value independent on disorder as long as the scattering rate is much smaller than the maximum SC gap Δ and vertex corrections can be ignored [37,38]. In the present paper we perform a systematic analysis of the linear and nonlinear current response as a function of lattice size, using the linear response also as a benchmark of the reliability of the numerical results even at small disorder down to frequencies well below Δ. Finite-size effects become instead irrelevant when the scattering rate becomes of the same order as Δ, so in this limit our calculated response is essentially valid down to $\omega = 0$. The results for the optical conductivity and the superfluid stiffness are in very good agreement with experimental data from cuprate superconductors [31,32]. In particular, in the disorder regime $2\Delta\tau \approx 1$ relevant for overdoped cuprates, our calculations support the relevance of out-of plane impurities for the vanishing of T_c and of the superfluid fraction.

For the THG our calculations show a marked qualitative difference with respect to the s-wave case. Indeed, while the general mechanism of a strong overall enhancement of paramagneticlike THG processes is confirmed, for d-wave pairing the response rapidly loses the resonance at 2Δ characteristic of the clean limit that is instead found to survive for s-wave superconductors up to strong disorder [25]. At the same time, disorder washes out the strong orientation dependence due to the diamagneticlike processes dominating the clean case, in analogy with the s-wave case. Both effects, i.e., the absence of a marked frequency resonance of $\chi^{(3)}$ at 2Δ and the smooth polarization dependence, are in good agreement with the recent experimental findings [11,14–16], as discussed above.

The paper is organized as follows. In Sec. II we discuss the model and how the disordered ground state solutions are obtained within the Bogoljubov–de Gennes approach. Section III presents the corresponding results for the optical conductivity that are discussed within the context of experiments on the superfluid density in overdoped cuprates. The influence of disorder on the third harmonic response and its dependence on the polarization of the incoming light is then analyzed in Sec. IV and we conclude our discussion in Sec. V. In Appendix A we give a detailed derivation on how we compute the linear and nonlinear current, Appendix B is devoted to an analysis of finite size effects, Appendix C discusses the evaluation of the universal conductivity for the parameters used in the present paper, and finally in Appendix D we report the estimate of the transport scattering time for the different disorder levels we used to evaluate the optical response.

II. MODEL AND FORMALISM

To model the d-wave SC order emerging in cuprates we consider a tight-binding model on a square lattice, with an interaction part modeled as intersite spin-spin ($\sim J$) interactions together with local on-site disorder (cf., e.g., Refs. [39–41])

$$H = \sum_{ij\sigma}(t_{ij} - \mu\delta_{ij})c^{\dagger}_{i\sigma}c_{j\sigma} + \sum_{i\sigma} V_i n_{i\sigma} + J\sum_{\langle ij\rangle}\left[\mathbf{S}_i\mathbf{S}_j - \frac{1}{4}n_i n_j\right], \quad (2)$$

where t_{ij} includes the hopping between nearest ($\sim t$) and next-nearest ($\sim t'$) neighbors, $\langle ij\rangle$ denotes the summation over nearest neighbors only, and $\mathbf{S}_i$ is the spin operator at lattice site R_i. V_i is a random variable taken from a flat distribution with $-V_0 \leqslant V_i \leqslant +V_0$.

In order to avoid any interference with competing phases, we neglect the decoupling of the interaction part with respect to on- ($i = j$) and intersite ($i \neq j$) charge densities $\langle c^\dagger_{i,\sigma} c_{j,\sigma}\rangle$. The mean-field Hamiltonian therefore reads

$$H^{MF} = \sum_{ij\sigma}(t_{ij} - \mu\delta_{ij})c^\dagger_{i\sigma}c_{j\sigma} + \sum_{i\sigma} V_i n_{i\sigma} \tag{3}$$

$$+\frac{1}{2}\sum_{i,\delta}[\Delta_{i,\delta}(c^\dagger_{i,\uparrow}c^\dagger_{i+\delta,\downarrow} + c^\dagger_{i+\delta,\uparrow}c^\dagger_{i,\downarrow}) + \Delta^*_{i,\delta}(c_{i,\downarrow}c_{i+\delta,\uparrow} + c_{i+\delta,\downarrow}c_{i,\uparrow})] + \frac{1}{J}\sum_{i,\delta}|\Delta_{i,\delta}|^2, \tag{4}$$

where

$$\Delta_{i,\delta} = -\frac{J}{2}[\langle c_{i,\downarrow}c_{i+\delta,\uparrow}\rangle + \langle c_{i+\delta,\downarrow}c_{i,\uparrow}\rangle] \tag{5}$$

represent a bond SC order parameter with $\delta \equiv \pm x, \pm y$.

A. Equilibrium solution

In equilibrium, in analogy with the well-studied s-wave case [25,42–47], the Hamiltonian Eq. (3) can be diagonalized by means of the Bogoliubov–de Gennes (BdG) transformation

$$c_{i\sigma} = \sum_k [u_i(k)\gamma_{k,\sigma} - \sigma v^*_i(k)\gamma^\dagger_{k,-\sigma}],$$

which yields the eigenvalue equations:

$$\omega_k u_n(k) = \sum_j t_{nj}u_j(k) + [V_n - \mu]u_n(k) + \sum_\delta \Delta_{n,\delta}v_{n+\delta}(k), \tag{6}$$

$$\omega_k v_n(k) = -\sum_j t_{nj}v_j(k) - [V_n - \mu]v_n(k) + \sum_\delta \Delta^*_{n,\delta}u_{n+\delta}(k). \tag{7}$$

In the following $u_i(k)$ and $v_i(k)$ are taken to be real. This excludes, e.g., ground states with circular currents which have been studied in models where disorder is implemented via a variable concentration n_i of scatterers with fixed impurity strength [35,48]. In our system with an Anderson type of disorder the calculations with complex $u_i(k)$ and $v_i(k)$ did not yield stable solutions at small and intermediate disorder. For large $V_0/t \sim 1$ we observe instabilities in the ground state (cf. Sec. V), which may be due to circular currents and which will be investigated in detail elsewhere.

Starting from an initial random distribution for the anomalous expectation values we diagonalize the system of equations (6) and (7) and iterate up to a given accuracy (10^{-8}) for the $\Delta_{i,\delta}$. In order to check the stability of the solution we also add random values to the iterated anomalous expectation values and check if a subsequent iteration converges to the same previous solution.

Results are obtained for a charge density $n = 0.875$ and all parameters are measured with respect to the nearest-neighbor hopping t. The exchange coupling is taken as $J/t = 1$ and we also include a next-nearest-neighbor hopping $t'/t = -0.2$, as appropriate for cuprates. For the homogeneous system one obtains a d-wave gap

$$\Delta_{\mathbf{k}} = \frac{\Delta}{2}[\cos(k_x) - \cos(k_y)], \tag{8}$$

with $\Delta/t = 0.316$ and thus a maximum optical gap 2Δ, which decreases upon including disorder. In cuprates, gap values extracted from angle-resolved photoemission (ARPES) on Bi2212 (see, e.g., Ref. [49]) can reach values $\Delta =$ 30–40 meV, which in our model would correspond to hopping values $t =$ 100–130 meV. This is compatible with our value for the exchange coupling $J/t = 1$ and even with tight-binding fits to the dispersion and Fermi surface as obtained by ARPES [50]. However, for other compounds the hopping is estimated to be in the range $t =$ 200–300 meV so that our investigations should be considered as a qualitative but not necessarily a quantitative prediction of the linear and nonlinear current response in cuprate superconductors.

B. Equations of motion for the density matrix to evaluate the response to a time-dependent vector potential

Denoting with ρ and κ the normal and anomalous averages,

$$\rho_{ij} = \langle c^\dagger_{i,\uparrow}c_{j,\uparrow}\rangle, \quad \bar\rho_{ij} = \langle c_{i,\downarrow}c^\dagger_{j,\downarrow}\rangle,$$
$$\kappa^\dagger_{ij} = \langle c^\dagger_{i,\uparrow}c^\dagger_{j,\downarrow}\rangle, \quad \kappa_{ij} = \langle c_{i,\downarrow}c_{j,\uparrow}\rangle,$$

the total density matrix can be defined as

$$\mathcal{R} = \begin{pmatrix} \rho & \kappa^\dagger \\ \kappa & \bar\rho \end{pmatrix}. \tag{9}$$

In the inhomogeneous systems it is represented by a $2L \times 2L$ matrix, with the lattice size L varying from 52 to 68 in our simulations. The equation of motion reads [51]

$$i\frac{d}{dt}\mathcal{R} = [\mathcal{R}, \mathcal{H}^{BdG}], \tag{10}$$

where the BdG Hamiltonian matrix can be derived from the BdG mean field energy as

$$\mathcal{H}_{ij} = \frac{\partial E^{BdG}}{\partial \mathcal{R}_{ji}} \tag{11}$$

and the latter is given by

$$E^{BdG} = -\sum_{ij} t_{ij}(\rho_{ij} - \bar\rho_{ij}) - \frac{J}{4}\sum_{\langle ij\rangle}\kappa^\dagger_{ij}\kappa_{ij} + \sum_i V_i(\rho_{ii} - \bar\rho_{ii} + 1).$$

In the absence of an external field the density matrix $\mathcal{R}$ and the Hamiltonian $\mathcal{H}^{BdG}$ commute, so it simply follows from Eq. (10) that the density matrix has no time evolution. The dynamics of $\mathcal{R}(t)$ is induced via the coupling to the electromagnetic field $\vec{E}(t) = -\partial\vec{A}(t)/\partial t$. Let us consider, e.g., the case of a (spatially constant) field along the x direction. $A_x(t)$ is coupled to the system via the Peierls substitution

$c^\dagger_{i+x,\sigma}c_{i,\sigma} \to e^{iA_x(t)}c^\dagger_{i+x,\sigma}c_{i,\sigma}$, where for simplicity we will drop from the equations all the constant by putting the lattice spacing, the electronic charge e, the light velocity c, and the Planck constant $\hbar$ equal to one. As one can easily check, the interaction terms in Eq. (2) are unaffected by the Peierls substitution, while the kinetic-energy part gets modified, leading to the following contribution to E^{BdG}:

$$\begin{aligned} T^{BdG} = &-t\{e^{iA_x}\rho_{i+x,i} + e^{-iA_x}\rho_{i-x,i} - e^{-iA_x}\bar{\rho}_{i+x,i} - e^{iA_x}\bar{\rho}_{i+x,i}\} \\ &- t'\{e^{iA_x}\rho_{i+x,i+y} + e^{-iA_x}\rho_{i-x-y,i} - e^{-iA_x}\bar{\rho}_{i+x+y,i} \\ &- e^{iA_x}\bar{\rho}_{i+x+y,i} + e^{iA_x}\rho_{i+x,i-y} + e^{-iA_x}\rho_{i-x+y,i} \\ &- e^{-iA_x}\bar{\rho}_{i+x-y,i} - e^{iA_x}\bar{\rho}_{i+x-y,i}\}. \end{aligned} \tag{12}$$

Writing $A_x(t) = A_0 f(t)$ one can now expand the density matrix and the Hamiltonian [i.e., the kinetic part resulting from Eq. (12)] in powers of A_0, i.e.,

$$\mathcal{R} = \sum_{n=0} A_0^n \mathcal{R}^{(n)}, \tag{13}$$

where $\mathcal{R}^{(0)}$ is the equilibrium density matrix for which

$$[\mathcal{R}^{(0)}, \mathcal{H}^{BdG}] = 0, \tag{14}$$

as we already emphasized above. The current density is obtained at all orders in A_x as $j_x = -(1/N)\frac{\partial E^{BdG}}{\partial A_x} = -(1/N)\frac{\partial T^{BdG}}{\partial A_x}$ with $N \equiv L^2$. Thus, by retaining terms up to third order in A_x, one has

$$j_x = \left(1 - \tfrac{1}{2}A_x^2\right) j^x_{para} + A_x\left(1 - \tfrac{1}{6}A_x^2\right) j^x_{\rm dia}, \tag{15}$$

with

$$\begin{aligned} j^x_{para} = &\, it \sum_n [\rho_{n+x,n} - \bar{\rho}_{n-x,n} - \rho_{n-x,n} + \bar{\rho}_{n+x,n}] \\ &+ it' \sum_n [\rho_{n+x+y,n} - \bar{\rho}_{n-x-y,n} - \rho_{n-x-y,n} + \bar{\rho}_{n+x+y,n}] \\ &+ it' \sum_n [\rho_{n+x-y,n} - \bar{\rho}_{n-x+y,n} - \rho_{n-x+y,n} + \bar{\rho}_{n+x-y,n}], \end{aligned} \tag{16}$$

$$\begin{aligned} j^x_{\rm dia} = &-t \sum_n [\rho_{n+x,n} - \bar{\rho}_{n-x,n} + \rho_{n-x,n} - \bar{\rho}_{n+x,n}] \\ &- t' \sum_n [\rho_{n+x+y,n} - \bar{\rho}_{n-x-y,n} + \rho_{n-x-y,n} - \bar{\rho}_{n+x+y,n}] \\ &- t' \sum_n [\rho_{n+x-y,n} - \bar{\rho}_{n-x+y,n} + \rho_{n-x+y,n} - \bar{\rho}_{n+x-y,n}]. \end{aligned} \tag{17}$$

Here the subscript *para* and *dia* refer to the usual identification of the leading terms coupling the gauge field to the fermionic operators in the Hamiltonian, i.e., the linear coupling between the paramagnetic term and A_x and a quadratic coupling between the electronic density and A_x^2, which leads to the standard diamagnetic contribution to the current in linear response. To make a closer connection to standard notation in Nambu operators for the SC state [17,19–24,27], the paramagnetic term is described by a τ_0 Pauli matrix and the diamagnetic term by a τ_3 matrix. Here the j^x_{para} and $j^x_{\rm dia}$ terms represent directly average values of such fermionic operators in the presence of the external gauge field and such are expressed in terms of the density-matrix elements ρ, which in turn contain the dependence on A_x at all orders. The expansion Eq. (13) therefore explicitly reads

$$j^x_{para} = \sum_n A_0^n j^{x,(n)}_{para}, \quad j^x_{\rm dia} = \sum_n A_0^n j^{x,(n)}_{\rm dia},$$

which upon inserting into Eq. (15) allows us to extract the various current contributions to order n, $j_x^{(n)}$.

In particular, the third harmonic contribution to the current density reads

$$j_x^{(3)} = j^{x,(3)}_{para} - \tfrac{1}{2}A_0^2 j^{x,(1)}_{para} + A_0 j^{x,(2)}_{\rm dia} - \tfrac{1}{6}A_0^3 j^{x,(0)}_{\rm dia}, \tag{18}$$

where we find that, similar to the isotropic s-wave case [25], the dominant para- and diamagnetic contributions are given by $j^{x,(3)}_{para}$ and $A_0 j^{x,(2)}_{\rm dia}$. On the other hand, $j^{x,(1)}_{para}$ and $j^{x,(0)}_{\rm dia}$ enter the calculation of the optical conductivity in first order. The explicit expressions for the nth order density matrix ($n = 1, 2, 3$), from which para- and diamagnetic current contributions can be obtained according to Eqs. (16) and (17), are given in Appendix A.

The consideration of disordered d-wave superconductors requires the investigation of large systems in order to capture the responses at low energies. Here we study lattices between 52×52 and 68×68, which allows us to elucidate the role of finite-size effects. On the other hand, due to the large system sizes it is not possible to include collective (SC amplitude, SC phase, and density) excitations on top of the BdG solution due to the much larger matrices required when interactions between quasiparticle excitations are taken into account within a random phase approximation. Therefore, the responses reflect the quasiparticle contributions only. The collective-mode contribution has been shown to become sizable in both the linear [44,52] and the nonlinear [25] response of strongly disordered s-wave superconductors. The accuracy of our calculations is determined by the ratio J/B, where $B \approx 8t$ denotes the bandwidth. For our parameters given above $J/B = 0.125 < 1$ and we will consider moderate levels of disorder only, so that we expect only a minor contribution of collective modes. In fact, preliminary calculations on small systems confirm this hypothesis which is also supported by the evaluation of the stiffness including phase fluctuations in Sec. III. Therefore, we will focus for the moment on the BCS response only, that is presumably the most relevant one in the underdoped and optimally doped regime of cuprates. For this reason, we implement here a different (and faster) procedure for evaluating the response functions with respect to our previous work [25,28], since instead of solving the time dependent density matrix for an arbitrary vector potential we directly truncate the equations of motion for each frequency at the desired order.

III. LINEAR RESPONSE AND SUPERFLUID STIFFNESS

The optical conductivity $\sigma(\omega) = \sigma_1(\omega) + i\sigma_2(\omega)$ for an applied electric field along $\mathbf{e}_x$ and the current response along the same direction is obtained from

$$\sigma_1(\omega) = \pi[-\langle t_x\rangle + \chi_1(\omega = 0)]\delta(\omega) - \frac{\chi_2(\omega)}{\omega}, \tag{19}$$

$$\sigma_2(\omega) = \frac{-\langle t_x\rangle + \chi_1(\omega)}{\omega}, \tag{20}$$

where $\chi_{1,2}$ are the real and imaginary parts of the current-current correlation function $\chi(\omega)$, respectively. Within our formalism, cf. Appendix A, $\chi(\omega)$ is obtained from $\chi(\omega) \equiv j^{(1)}_{para}(\omega)$ and $\langle t_x \rangle \equiv j^{(0)}_{\rm dia}$, where in general $j^{(n)}_{para/dia}$ refers to the nth term in the expansion in powers of the gauge field of the paramagnetic or diamagnetic electronic current. Since the diamagnetic current response is already linear in the gauge field, the zeroth term is sufficient to compute the linear response. We set $\hbar = e = a \equiv 1$ so that the conductivity in these units is dimensionless and should be multiplied by $e^2/\hbar$ in order to obtain a two-dimensional $\sigma(\omega)$ in SI units. In order to obtain the three-dimensional $\sigma(\omega)$ for layered cuprates one should multiply the dimensionless conductivity times $e^2/(\hbar d)$, with d denoting the interlayer spacing.

Figure 1 reports real and imaginary parts of the optical conductivity obtained from averages over disorder configurations (10–20 samples) and averages over system sizes from 52×52 to 68×68; see also discussion below. Here blue solid lines denote results in the SC state at $T = 0$, while red dashed lines denote results at $T = 0$ in the absence of SC order. On finite lattices and for a given particle number the chemical potential μ does not necessarily coincide with an available quasiparticle energy ε_k, so the minimum gap for a d-wave superconductor $E_k = \sqrt{(\varepsilon_k - \mu)^2 + \Delta_k^2}$ can be different from zero also along the nodal direction. As shown in Appendix B, for a clean system this minimum gap is an oscillatory function of the system size N. Clearly also the low-energy density of states depends on N. Nonetheless, this spurious effect can be removed by performing an additional average over systems of different sizes, as shown explicitly in Appendix B in the homogeneous case. The gray region in Fig. 1 indicates the spread of the results due to the evaluation on different lattice sizes. For disorder values up to $V_0/t = 0.5$ it can be seen that finite-size effects become relevant in the real part of the optical conductivity for frequencies below $\omega \sim 0.25t$, whereas they have only minor influence on $\sigma_2(\omega)$. In the strong disorder limit $V/t = 1.0$ finite-size effects are no longer relevant, so that we can consider the results reliable down to $\omega = 0$ in this case.

To better quantify the disorder strength we estimate the dimensionless quantity $2\Delta\tau$, where Δ is the gap maximum obtained for each disorder level from the maximum in the density of states and τ is the normal-state transport scattering time. To this aim we extract τ from an analysis of the normal-state conductivity, as outlined in Appendix D. In general, by increasing disorder (i.e., by decreasing $2\Delta\tau$), one observes an enhancement of $\sigma_1(\omega)$ in the frequency range below 2Δ, as due to the increase of the paramagnetic current response [$\chi_2(\omega)$ in Eq. (19)], see Figs. 1(a), 1(c), 1(e), and 1(g), similar to previous theoretical studies [34–36]. For a d-wave superconductor it has been shown [37] that the conductivity approaches a so-called universal value $\sigma_0 = \lim_{\omega\to0} {\rm Re}\sigma(\omega, T = 0) \approx e^2 N_\sigma v_F^2 \hbar/(\pi\Delta)$ for weak disorder, irrespective of the disorder model. Here N_σ is the DOS per spin at the Fermi level in the normal state, v_F is the Fermi velocity, and the order parameter has the d-wave angular dependence $\Delta(\mathbf{k}_F) = \Delta\cos(2\phi)$ on the Fermi surface in the clean case. In Appendix C we evaluate σ_0 for the parameters of our model showing that $\sigma_0 = 2.38[e^2/\hbar]$ in the weak-disorder limit. On the other hand, as disorder increases σ_0 is no longer universal and its value depends on the disorder realization. We used the approach of Ref. [53] to estimate $\sigma_0 = 0.6[e^2/\hbar]$ in the strong-disorder unitary limit for our parameter values. These two limiting analytical values can be compared with the numerical estimates of Fig. 1. As mentioned above, for weak to moderate disorder our values of $\sigma_1(\omega \to 0)$ are subject to errors due to finite-size effects. Nonetheless, at $V/t = 0.5$–0.7 the numerical σ_0 compares well with its expected thermodynamic value within the uncertainty of the calculation [denoted by the gray area in Figs. 1(a) and 1(b)]. In addition, our calculations indicate a low-energy increase of $\sigma_1(\omega)$, i.e., the tendency for

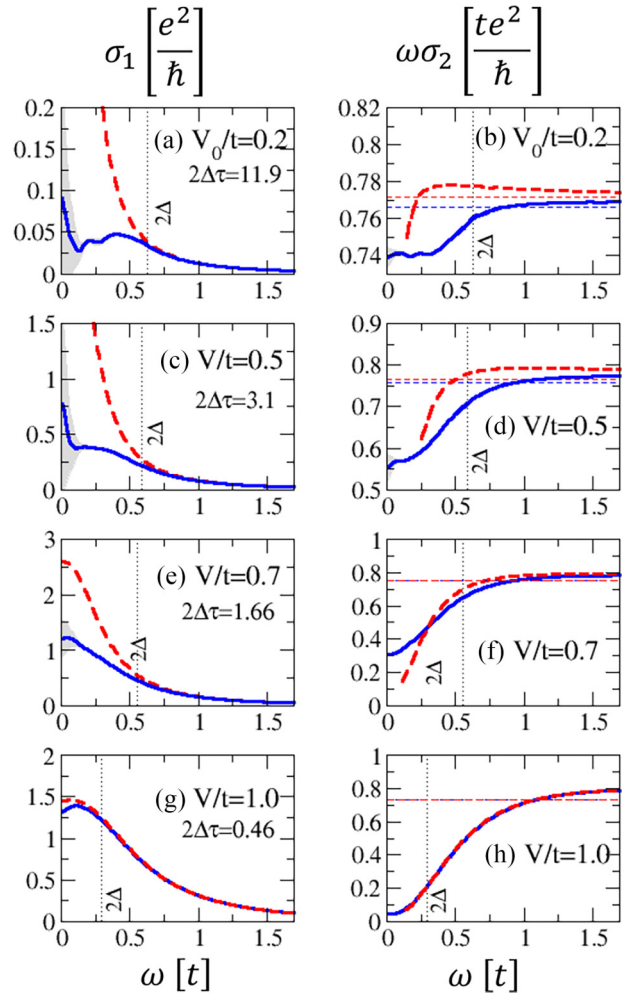

FIG. 1. Optical conductivity at $T = 0$ in the SC state (blue solid line) and in the non-SC state (red dashed line) for increasing disorder, as indicated in the panels. Panels (a), (c), (e), and (g) show the real part σ_1, and panels (b), (d), (f), and (h) show the product $\omega\sigma_2$ with σ_2 imaginary part. The limit $\omega \to 0$ of $\omega\sigma_2$ identifies the superfluid stiffness, while its high-frequency limit coincides with $-\langle t_x \rangle$, that is weakly disorder dependent. Here we used $J/t = 1$, $n = 0.875$, $t'/t = -0.2$, and we averaged over different lattice sizes from 52×52 to 68×68. The variance with regard to the different lattice sizes is indicated by the gray shaded areas. A Lorentzian broadening (cf. Appendix A 1) $\eta = 0.02t$ has been used. The vertical dotted lines indicate the maximum spectral gap 2Δ extracted from the density of states.

approaching the universal value σ_0. At strong disorder, where our results for $\omega \to 0$ become reliable, we obtain a somehow larger universal conductivity than what is estimated from the perturbative scheme of Ref. [53], which is expected to fail in this strong-disorder limit. Our calculations also indicate a slight downturn upon approaching $\omega \to 0$, which in the strongly disordered regime [54] develops towards a peak at $\omega \sim 1/\tau$. In the regime $2\Delta\tau < 1$ we also observed the formation of SC islands, similar to the case of strongly disordered s-wave SCs [42–47].

Panels (b), (d), (f), and (h) of Fig. 1 report $\omega\sigma_2(\omega) = -\langle t_x\rangle + \chi_1(\omega)$ for the various disorder levels. At large frequencies (larger than the bandwidth) $\chi_1(\omega) \sim 1/\omega$, so that $-\langle t_x\rangle$ identifies the large-frequency behavior of $\omega\sigma_2(\omega)$. In addition, since $-\langle t_x\rangle$ has very small changes when going from the normal to the SC state, the asymptotic values are pretty much similar in the two cases, as one can see by comparing solid blue and dashed red lines. In contrast, in the limit $\omega \to 0$ this quantity corresponds to the superfluid stiffness $D_s \equiv \lim_{\omega\to 0} \omega\sigma_2(\omega)$, which is finite in the SC case but vanishes in the metallic state. In general the stiffness is reduced with increasing disorder from its clean value $-\langle t_x\rangle$ due to the paramagnetic current response $\chi_1(\omega = 0)$. At strong disorder the superfluid stiffness is almost completely suppressed [see panel (h)], consistent with the observation of a large fraction of uncondensed spectral weight in $\sigma_1(\omega)$ [see panel (g)].

Our results can be compared with experiments on overdoped LSCO films [31], which are in the range $0.31 \lesssim 2\Delta\tau \lesssim 2.45$, and overdoped LSCO films, which have been additionally exposed to ion irradiation [32] leading to even smaller values of $2\Delta\tau$. These measurements of $\sigma_1(\omega)$ have revealed that a large fraction of the carriers remains uncondensed in a wide Drude-type feature at low temperatures which resembles the $\sigma_1(\omega)$ in panels, e.g., of Fig. 1. A similar residual $\sigma_1(\omega \to 0)$ at low temperatures has also been observed in Bi2212 thin films [55].

To better quantify this effect we follow the same procedure adopted in the experiments [31,32], by reporting the SC fraction S_{sc}, found in the SC state as a δ-like peak in σ_1 at $\omega = 0$, of the total normal-state optical spectral weight S_n. By the so-called f-sum rule $S_n = \int_0^\infty d\omega\, \sigma_1(\omega) = -\pi/2\langle t_x\rangle$, while S_{sc} can be derived from Eqs. (19) and (20), as given by

$$S_{sc} = \frac{\pi}{2}[\langle t_\alpha\rangle + \chi_1(0)] = \frac{\pi}{2}\lim_{\omega\to 0} \omega\sigma_2(\omega). \qquad (21)$$

The ratio S_{sc}/S_{sn} is plotted as a function of $1/(2\Delta\tau)$ in Fig. 2, together with the corresponding data from Refs. [31,32]. Given the uncertainty in determining the various quantities (e.g., in Ref. [32] the SC gap has been estimated by means of the weak-coupling expression [56] for the ratio Δ/T_c) the agreement is rather remarkable. One could speculate that our model of Anderson-type impurities, where at each lattice site the local potential is taken from a random distribution, is more appropriate for the irradiated samples where the ions affect the electronic structure of the CuO_2 planes on a local scale. On the other hand, the disorder from the "unirradiated" data [31] is presumably mainly due to out-of plane dopant ions which impose a potential with a finite range on the in-plane charge carriers [57]. In view of these considerations it is interesting that the stiffness obtained in Refs. [31,32] follows nonetheless

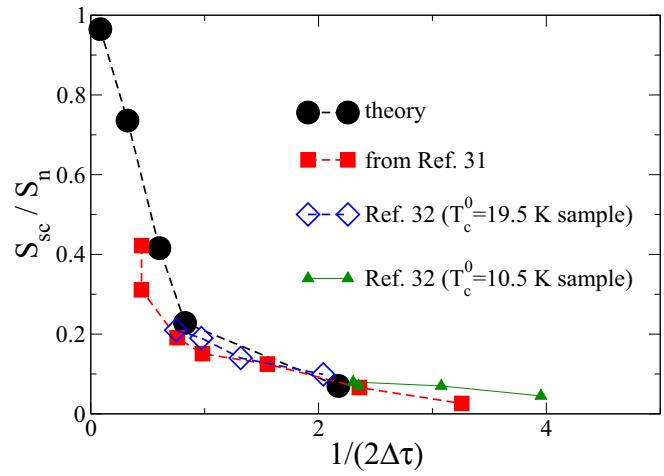

FIG. 2. Disorder dependence of the ratio S_{sc}/S_n between the superfluid δ-like peak in $\sigma_1(\omega)$ and the total optical spectral weight S_n in the SC state. Our numerical estimates (black dots) are compared with the experimental results from Refs. [31,32].

a similar disorder dependence, which is well captured by our model.

The present calculations of the linear optical response do not include fluctuations effects that have been shown to be relevant in the strongly disordered regime for s-wave superconductors [25,44,52]. As it is well known [58], phase fluctuations are crucial to restore the gauge invariance violated by the BCS approximation of the response functions. However, in the clean limit they do not affect the value of the superfluid stiffness, since their correction is purely longitudinal. In the disordered case the longitudinal and transverse response become mixed and a full gauge-invariant calculation of the stiffness [44] in the disordered s-wave case has shown that phase fluctuations lead to a further suppression of D_s as compared to the BCS suppression, along with a pileup of additional finite-frequency optical absorption below the optical gap [52], analogous to the one shown in Fig. 1. While a full computation of $\sigma(\omega)$ adding fluctuations effects is numerically challenging for the large lattice sizes used so far, we can nonetheless analyze the static limit of the fluctuations-induced suppression of D_s, following an approach analogous to the one employed in Ref. [44]. We thus add a small $\mathcal{O}(10^{-3})$ vector potential in the Hamiltonian Eq. (2) via the Peierls substitution and we compute D_s by taking the ratio between the total current and the vector potential. To this aim, in order to guarantee the conservation of the total (dia- plus paramagnetic) current at each node, one has to introduce a complex value of the local order parameter. Indeed, one finds that not only are the local amplitudes $|\Delta_{i,\delta}|$ affected, but more importantly the local phases are needed to guarantee locally the continuity equation, that is instead violated by the (non-gauge-invariant) BCS approximation, corresponding to the evaluation in the absence of local-phase relaxation; see Ref. [44].

Figure 3 compares the stiffness, obtained via this gauge-invariant approach, with the corresponding BCS result on a logarithmic (main panel) and linear (inset) scale. We find that for the present parameters fluctuation corrections up to $V_0/t = 0.7$ are small (~5% at $V_0/t = 0.7$), whereas at $V_0/t = 1.0$ the

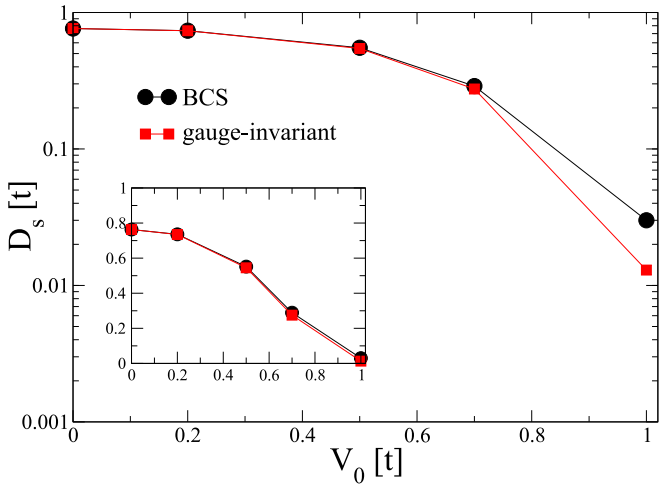

FIG. 3. Superfluid stiffness S_{sc} as a function of disorder from Eq. (21) evaluated in the BCS (black) and gauge-invariant (red) approach.

BCS stiffness overestimates the gauge-invariant result by a factor ∼2.

We point out that a reduction of D_s due to fluctuation effects has a significantly stronger impact on the optical conductivity for the isotropic s-wave case rather than for the d-wave symmetry. Indeed, the f-sum rule dictates that the decrease in D_s, entering the S_n spectral weight of Eq. (21), has to be compensated by an increase in $\sigma_1(\omega)$. In a fully gapped s-wave superconductor with a hard gap at 2Δ collective excitations occur mainly below 2Δ. These can induce a subgap absorption below the gap as described in [52]. On the other hand, in a d-wave superconductor quasiparticle excitations already contribute considerably to absorption below 2Δ, so that the collective-mode contribution only results in a minor redistribution of the finite spectral weight at low energies.

It should be noted that at strong disorder $V_0/t = 1.0$ and upon including fluctuations our calculations reveal a *negative* stiffness for a significant number of disorder realizations. Such samples have been then excluded from the average procedure leading to the results shown in Fig. 3. A value $D_s < 0$ in principle means that the considered solution does *not* correspond to the true ground state since the free energy as a function of the vector potential would have a negative curvature. In fact, for smaller systems, where an RPA analysis is possible, samples with a negative stiffness also lack a well-defined zero energy Goldstone mode. The latter instead is replaced by a strongly overdamped feature indicating that the iteration of the BdG equations has converged to an unstable solution. In principle, the instability could also arise from the fact that we have restricted to real valued order parameters which excludes solutions such as circular currents [35,48]. Although preliminary investigations have not provided any evidence for the existence of such currents within our model, we cannot exclude that there may exist solutions with lower energy which are made from complex BdG amplitudes.

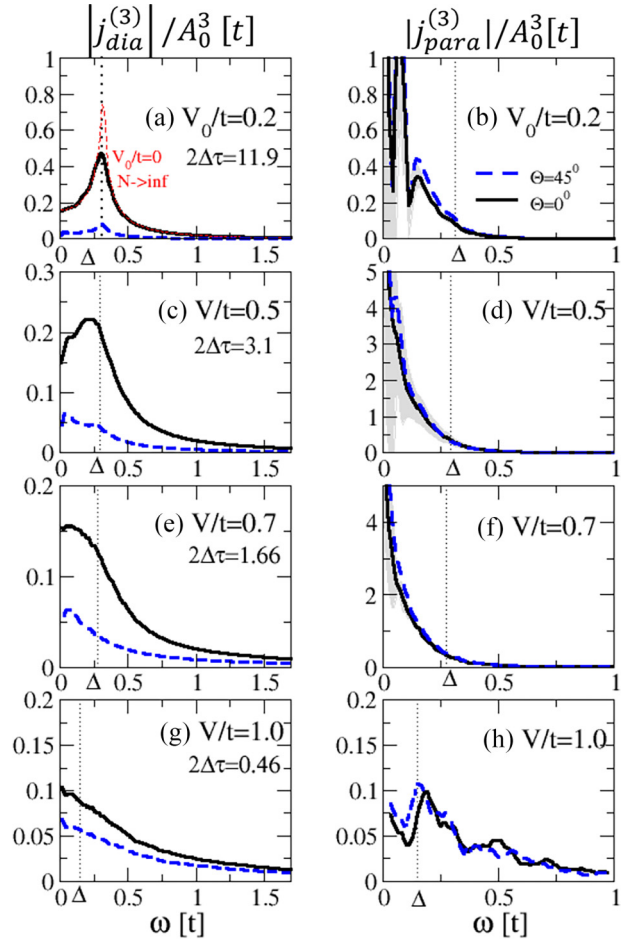

FIG. 4. Diamagnetic (left column) and paramagnetic (right column) contributions to the third-harmonic current at various disorder levels obtained from averages over different lattice sizes from 52×52 to 68×68. The variance with regard to the different lattice sizes is indicated by the gray shaded areas. Solid black and blue dashed lines refer to the response for a field applied along the [10] and [11] direction, respectively. In panel (a) we also report for comparison the analytical results (22) of the [10] clean case, obtained for an infinite-size system. Parameter values are the same as in Fig. 1.

IV. THIRD HARMONIC GENERATION

As it has been widely discussed in previous work both for clean [17,19,20,24] and disordered [21–23,25,27,28] superconductors, the THG can be computed within a diagrammatic approach or within a density-matrix formalism by computing all third-order processes arising from paramagneticlike or diamagneticlike coupling terms between the gauge field A and the fermions, the former being linear and the latter quadratic in A. In full analogy, as detailed in Appendix A, we decompose the third-harmonic current in a diamagnetic and paramagnetic contribution $j_{dia/para}(3\omega)$, both computed at finite gauge field and retaining up to third order in A. Since we are interested in the THG measured experimentally with a multicycle pump field, we study the nonlinear response to a harmonic vector potential $A(t) = A_0 \cos(\omega t)$. In Fig. 4 we report the magnitude of both responses $|j_{dia/para}(3\omega)/A_0^3|$ for the various disorder levels. We found that these responses are only finite, within

our numerical accuracy, in the SC state. As for the optical conductivity, we have analyzed finite-size effects which are mainly relevant for the third-harmonic paramagnetic response in the limit of weak to moderate disorder and low frequencies [cf. panel (b), where the variance is indicated by the gray region].

In the clean limit the third-harmonic paramagnetic current in response to a monochromatic field at ω vanishes [19,20] and THG is only controlled by the diamagnetic response,

$$j^{(3)}_{\mathrm{dia,clean}}(3\omega)/A_0^3 = \frac{1}{N}\sum_k \frac{\Delta_k^2}{E_k}\frac{4\left(t_k^x\right)^2}{4\omega^2 - 4E_k^2}, \qquad (22)$$

whose value in the limit $N \to \infty$ is also plotted for comparison with a red dashed line in Fig. 4. The $j^{(3)}_{\mathrm{dia,clean}}$ corresponds to a densitylike correlation function with a diamagnetic vertex [19]. We consider the response along the [10] direction ($\equiv x$) so that the vertex is determined by the derivatives of the kinetic energy [i.e., the Fourier transform of the hopping term in Eq. (2)] along the x direction $t_k^x = \partial^2\varepsilon_k/\partial k_x^2$ [19,24].

In the d-wave case the logarithmic singularity of $j^{(3)}_{\mathrm{dia,clean}}$ at $\omega = \Delta$ in Eq. (22) is responsible for the strong enhancement of the THG when $\omega = \Delta$, in full analogy with the result of the clean s-wave case [19]. A strong enhancement is still retained by the diamagnetic response at weak disorder, even though, similar to the isotropic s-wave case [25], it broadens and decreases with increasing disorder. Also in analogy with the isotropic s-wave case the diamagnetic current displays a strong orientational dependence. In Fig. 4 the blue dashed (black solid) line corresponds to j_{dia} along the [11] ([10]) direction with the field applied along the same orientation. The suppression of the response along the [11] direction is most pronounced for weak disorder: For $2\Delta\tau = 11.9$ one finds a factor of $\approx$6 between the currents along the [10] and [11] direction. In the case of $2\Delta\tau = 0.46$ this value is reduced to $\approx$1.5.

The paramagnetic current [Figs. 4(b), 4(d), 4(f), and 4(h)], absent in the clean case for the same mechanism valid for s-wave superconductors [19,24], becomes finite as soon as even a weak disorder is included. However, in sharp contrast with the disordered s-wave case [21–23,25], it does not retain any resonant behavior around the gap maximum $\omega = \Delta$, but it shows instead a finite value below $\omega \approx \Delta$, with a continuous increase toward lower energies. Once more, due to finite-size effects we cannot explore the limit $\omega \to 0$ at weak to moderate disorder. However, the general trend of our results shows an increase of the paramagnetic response with disorder up to $2\Delta\tau \approx 1$, which then is followed by a decrease in the limit of strong disorder. In contrast to the diamagnetic current the orientational dependence of j_{para} is weak at any disorder level, with almost no dependence within the range of the numerical error. This results is also consistent with previous work for the same band structure and s-wave pairing [28], suggesting that the pairing symmetry plays a minor role in determining the polarization dependence of the THG response.

The dramatic increase of the response at low energies together with the absence of a clear resonance in the paramagnetic response represents a marked qualitative difference with respect to the s-wave case, where instead the paramagnetic current follows the diamagnetic response and is enhanced around $\omega = \Delta$ [21,25]. This theoretical result is in agreement with the experimental observation on, e.g., conventional s-wave superconductors such as NbN [5] and MgB_2 [8,9], where the presence of a frequency maximum in the nonlinear kernel $\chi^{(3)}$ can be traced back to an enhancement of the THG measurements at the temperature where the pump frequency ω matches the SC gap $\Delta(T)$. Interestingly, such a maximum has not been reported so far in most measurements on d-wave cuprate superconductors [11,12,14–16]. One possible interpretation for the lack of a temperature resonance is that in cuprates the SC gap is significantly larger than in conventional superconductors ($\Delta \sim 30$–40 meV) [49]. Thus multicycle pulses with central frequency ranging from $\omega = 0.5$ to $\omega = 0.7$ THz, as the ones used so far, allow one to fulfill the resonance condition only very near to T_c, where the SC response is suppressed. On the other hand, the present calculations showing a rather featureless paramagnetic contribution can explain why for d-wave superconductors the nonlinear response loses a clear trace of the SC gap value, in contrast to what is found for s-wave superconductors. For example, the experimental data from Ref. [59] indicate a disorder level $2\Delta\tau \approx 1.2$, where our results [cf. Fig. 4, panel (f)] show a continuously increasing paramagnetic response towards lower energy dominating over the diamagnetic one. Translated into a temperature dependent response via $\Delta(T)$, one would then expect a continuously decreasing THG which vanishes close to T_c, which is in agreement with the THG data of Refs. [11,14,15].

Our theoretical findings are also in excellent agreement with the mild polarization dependence of the THG signal measured experimentally in cuprate superconductors [11,12,14,15]. Previous work [28] already showed that the inclusion of a next-nearest-neighbor hopping t' into the band structure already enhances the isotropy even for s-wave pairing. Here the effect is even stronger and from Fig. 4 it is evident that for a d-wave superconductor an orientational dependence is only expected for the diamagnetic response. However, at small frequencies and in the presence of disorder the diamagnetic response is completely exceeded by the paramagnetic current, which is almost isotropic. Figure 5 summarizes our results showing the nonlinear current intensity at two frequency values $\Omega = \Delta$ [panel (a)] and $\Omega = \Delta/2$ [panel (b)]. Whereas in the former case dia- and paramagnetic contributions to the THG are comparable, also in strong contrast to the s-wave case [25], it is apparent that for smaller frequencies and $1/(2\Delta\tau) \approx 1/2$ the orientational-dependent diamagnetic current gives only a minor contribution to the response. Since for cuprates one is well below the gap maximum for a wide temperature range, our results are pretty much consistent with an isotropic THG signal increasing monotonically below T_c. Interestingly, despite the lack of a clear signature of the gap maximum in the THG intensity as a function of frequency, preliminary investigations of the phase of the THG response suggest that this quantity could still be sensitive to the crossing at the $\omega = \Delta$ condition. The investigation of this issue will be left for future work.

V. CONCLUSIONS

In the present manuscript we performed a detailed analysis of the linear and nonlinear optical response for a model system

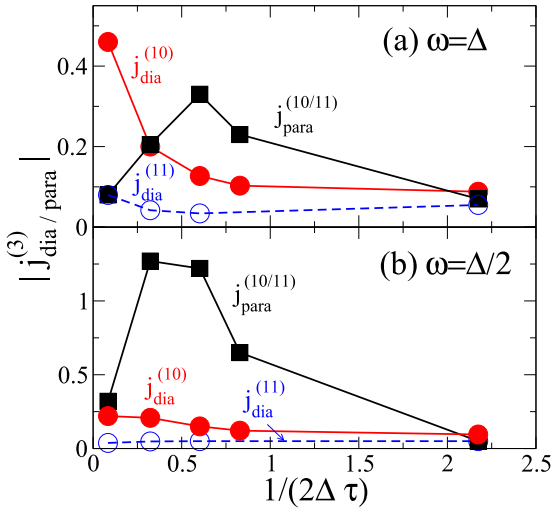

FIG. 5. Disorder dependence of the diamagnetic (circles) and paramagnetic (squares) response at two fixed frequencies $\omega = \Delta_0$ (top) and $\omega = \Delta_0/2$ (bottom). For the diamagnetic response we report the nonlinear current in the field direction for a field applied along the (11) (blue) and (10) (red) direction. For the paramagnetic current the value is the same within the numerical accuracy.

of d-wave superconductors, intended to reproduce the main features of cuprate superconductors in the SC state. Since strong correlation effects have not been explicitly included, our analysis is more appropriate for optimally and overdoped samples, even though general aspects concerning symmetry and disorder also apply to underdoped systems.

The linear response that has been widely studied in the past with various analytical and numerical approaches [34–36] provides a benchmark to test the accuracy of our results. Indeed, for a d-wave superconductor the vanishing of the gap along the nodal directions that is the origin [37] of the so-called universal value σ_0 of the optical conductivity in the limit $\omega \to 0$ makes it challenging to provide a reliable estimate of the zero-frequency limit at small disorder. Nonetheless, we show that our approach, based on the numerical solution of the self-consistent BdG equations and on a perturbative expansion in the applied gauge field, allows us to reproduce with good accuracy the expected value of σ_0 and the persistence of a large uncondensed fraction of optical spectral weight at larger disorder, recently reported in overdoped samples [31,32].

For what concerns the nonlinear optical response we focused on the third-harmonic current generated in response to a monochromatic gauge field that has been recently experimentally studied by different groups in various families of cuprates [11,14–16]. In analogy with previous work for s-wave superconductors [25], we show that even for small disorder the THG response is strongly enhanced, thanks to the emergence of a nonlinear coupling to light mediated by paramagneticlike processes that are absent in the clean case. However, in contrast to the s-wave case, the paramagnetic response, which rapidly dominates over the diamagnetic one already for relatively small disorder as appropriate for cuprates, completely loses any resonance in frequency at the scale set by the SC gap maximum Δ. When the system is probed at a fixed pump frequency with varying temperature, this result would imply a lack of any THG resonance in temperature when cooling below T_c. Our finding, along with the marked isotropy of the THG found in our calculations, bears a strong resemblance to the experimental data in cuprates, where no clear resonance in temperature of the THG has been reported [11,14–16].

So far, we only computed the BCS response due to quasiparticle excitations. Indeed, the large system sizes needed to correctly deal with the zero-frequency limit make it numerically challenging computing also the collective-mode response, as was done for the s-wave case [25]. It then remains a main open question regarding the fate of the Higgs mode, which in the strongly disordered s-wave case has been found to give a significant (but not predominant at intermediate disorder) contribution to the THG. So far, the analogy with the s-wave case led many authors to interpret also the THG data in cuprates as a signature of the Higgs mode [11,12,14,15], using as a main argument the isotropy of the signal as a function of the polarization dependence of the pump. However, the present calculations show clearly, as already anticipated for the same band structure and s-wave pairing [28], that for disorder values consistent with the available experimental results the paramagnetic response due to BCS quasiparticles correctly reproduces the measured isotropy of the THG. In addition, as discussed above, the lack of a resonance in the d-wave paramagnetic response could also explain the lack of a temperature maximum in the THG measured so far, showing that for the relatively clean underdoped and optimally doped samples the BCS response could very well explain the experiments. For what concerns the temperature dependence, a remarkable exception is provided by recent measurements in an optimally doped YBCO sample [14], where a broad maximum in THG is actually reported near T_c. Interestingly, for the same sample the time trace of the nonlinear current also shows a marked beating effect that seems to be ascribed to an interference effect between two well-defined sharp modes, in analogy with what observed, e.g., in $NbSe_2$ [60], where the Higgs mode coexists with a CDW amplitude mode. A possible interpretation of these results could be that, along with a featureless BCS paramagnetic response, also a subleading resonant Higgs contribution arises that becomes visible only when the resonance condition $\omega \approx \Delta$ is reached near T_c. Indeed, one could expect that at least for moderate disorder the main effect of impurities is to enhance the overall coupling of the Higgs mode to light, preserving its frequency structure with the same broad resonance at 2Δ found in the clean case [24]. In this view, even if subleading the Higgs mode could manifest whenever the matching condition with the pump frequency or with a coupled resonance makes it overcome the overall BCS signal. If confirmed, such a view could finally open the way to a detection mechanism able to disentangle the Higgs response from the BCS quasiparticle one and to investigate its role on the long-sought unconventional pairing mechanism at play in cuprate superconductors.

ACKNOWLEDGMENTS

We acknowledge financial support by ERC under the project MORE-TEM ERC-SYN (Grant Agreement No.

951215) and by Sapienza University of Rome under projects Ateneo 2021 (Grant No. RM12117A4A7FD11B) and Ateneo 2022 (Grant No. RP1221816662A977). The work of G.S. is supported by the Deutsche Forschungsgemeinschaft under Grant No. SE 806/20-1.

APPENDIX A: POWER SERIES EXPANSION FOR THE DENSITY MATRIX

In Sec. II B we have outlined a "real space scheme" to evaluate the deviation of the density matrix from its equilibrium result when the system is perturbed by the coupling to a time dependent vector potential. This approach is based on the equation of motion of the density matrix which allows for the evaluation of linear and nonlinear current responses for large lattices. We restrict the formalism to the BCS limit, i.e., keeping the local densities and order parameter values constant upon perturbing the system. In the following we give the explicit expressions for the nth order contributions to the density matrix $\mathcal{R}^{(n)}$ with $n = 1, 2, 3$ from which the para- and diamagnetic currents $j^{x,(n)}_{para/dia}$ of the same order can be computed according to Eqs. (16) and (17). Inserting these currents into Eq. (18) yields the full third harmonic current response.

1. First order

The first order current contribution, relevant for the evaluation of the optical conductivity, is given by

$$j_x^{(1)} = j^{x,(1)}_{para} + A_0 j^{x,(0)}_{\rm dia}, \tag{A1}$$

which requires evaluation of the density matrix up to order $n = 1$.

By selecting all terms $\sim A_0$ in the equation of motion Eq. (10) one obtains

$$i\underline{\underline{\dot{R}}}^{(1)} = [\underline{\underline{R}}^{(1)}, \underline{\underline{H}}^{(0)}] + f(t)[\underline{\underline{R}}^{(0)}, \underline{\underline{V}}], \tag{A2}$$

with

$$\underline{\underline{V}} = \begin{pmatrix} \underline{\underline{v}} & \underline{\underline{0}} \\ \underline{\underline{0}} & \underline{\underline{v}} \end{pmatrix} \tag{A3}$$

and

$$\begin{aligned} v_{nm} = &-it[\delta_{m,n+x} - \delta_{m,n-x}] \\ &- it'[\delta_{m,n+x+y} - \delta_{m,n-x-y}] \\ &- it'[\delta_{m,n+x-y} - \delta_{m,n-x+y}]. \end{aligned} \tag{A4}$$

The nonperturbed Hamiltonian $\underline{\underline{H}}^{(0)}$ (i.e., for $A_0 = 0$) can be diagonalized

$$\underline{\underline{\tilde{H}}}^{(0)} = \underline{\underline{T}}^{-1}\underline{\underline{H}}^{(0)}\underline{\underline{T}} = \begin{pmatrix} -E_N & \dots & 0 & 0 & \dots & 0 \\ \vdots & \ddots & 0 & \vdots & \dots & \vdots \\ 0 & \dots & -E_1 & 0 & \dots & 0 \\ 0 & \dots & 0 & E_1 & \dots & 0 \\ \vdots & & \vdots & \vdots & \ddots & \vdots \\ 0 & \dots & 0 & 0 & \dots & E_N \end{pmatrix}$$

and the same transformation also diagonalizes the nonperturbed density matrix

$$\underline{\underline{\tilde{R}}}^{(0)} = \underline{\underline{T}}^{-1}\underline{\underline{R}}^{(0)}\underline{\underline{T}} = \begin{pmatrix} 1 & \dots & 0 & 0 & \dots & 0 \\ \vdots & \ddots & 0 & \vdots & \dots & \vdots \\ 0 & \dots & 1 & 0 & \dots & 0 \\ 0 & \dots & 0 & 0 & \dots & 0 \\ \vdots & & \vdots & \vdots & \ddots & \vdots \\ 0 & \dots & 0 & 0 & \dots & 0 \end{pmatrix}.$$

With this transformation Eq. (A2) can be written as

$$i\dot{\tilde{R}}^{(1)}_{nm} = (E_{mm} - E_{nn})\tilde{R}^1_{nm} + \left(\tilde{R}^0_{nn} - \tilde{R}^0_{mm}\right)\tilde{V}_{nm} f(t), \tag{A5}$$

where $\underline{\underline{\tilde{V}}}$ denotes the transformed matrix Eq. (A3).

Consider now a harmonic vector potential $f(t) = \cos\Omega t$. Then the Fourier transformed correction

$$\tilde{R}^1_{nm}(\omega) = \int dt\, e^{i\omega t}\tilde{R}^1_{nm}(t) \tag{A6}$$

is given by

$$\begin{aligned} \tilde{R}^1_{nm}(\omega) &= \frac{\tilde{R}^0_{nn} - \tilde{R}^0_{mm}}{\omega - E_{mm} + E_{nn}}\tilde{V}_{nm}\pi[\delta(\omega - \Omega) + \delta(\omega + \Omega)] \\ &\equiv \tilde{\chi}_{nm}(\omega)\tilde{V}_{nm}\pi[\delta(\omega - \Omega) + \delta(\omega + \Omega)], \end{aligned} \tag{A7}$$

which can be transformed back to yield the first order perturbation $R^{(1)}_{ij}$ to the density matrix in the original site representation. For the presentation of the results in Sec. III, $\tilde{\chi}_{nm}(\omega \to \omega - i\eta)$ has been computed with a small imaginary part in order to avoid singularities.

2. Second order

We proceed by evaluating the diamagnetic contribution to the third harmonic current $A_0 j^{x,(2)}_{\rm dia}$; cf. Eq. (18). Collecting all terms $\sim A_0^2$ we find for the correction to the density matrix in second order

$$\begin{aligned} i\underline{\underline{\dot{R}}}^{(2)}(t) = &[\underline{\underline{R}}^{(2)}(t), \underline{\underline{H}}^{(0)}] + [\underline{\underline{R}}^{(1)}(t), \underline{\underline{V}}]f(t) \\ &+ \tfrac{1}{2}[\underline{\underline{R}}^{(0)}, \underline{\underline{C}}]f^2(t), \end{aligned} \tag{A8}$$

where we have defined the matrix

$$\underline{\underline{C}} = \begin{pmatrix} \underline{\underline{c}} & \underline{\underline{0}} \\ \underline{\underline{0}} & -\underline{\underline{c}} \end{pmatrix} \tag{A9}$$

and

$$\begin{aligned} c_{nm} = &\, t[\delta_{m,n+x} + \delta_{m,n-x}] + t'[\delta_{m,n+x+y} + \delta_{m,n-x-y}] \\ &+ t'[\delta_{m,n+x-y} + \delta_{m,n-x+y}]. \end{aligned} \tag{A10}$$

Fourier transformation yields

$$\begin{aligned} \omega\underline{\underline{R}}^{(2)}(\omega) = &[\underline{\underline{R}}^{(2)}(\omega), \underline{\underline{H}}^{(0)}] + \frac{1}{2}[\underline{\underline{R}}^{(1)}(\omega+\Omega) + \underline{\underline{R}}^{(1)}(\omega-\Omega), \underline{\underline{V}}] \\ &+ [\underline{\underline{R}}^{(0)}, \underline{\underline{C}}]\frac{\pi}{2}\left\{\delta(\omega) + \frac{1}{2}[\delta(\omega+2\Omega) + \delta(\omega-2\Omega)]\right\}, \end{aligned} \tag{A11}$$

which upon inserting Eq. (A7) and diagonalizing can be solved for the second order contribution to the density matrix as

$$\tilde{R}^2_{nm}(\omega) = \frac{\pi}{2}\tilde{\chi}_{nm}(\omega)\tilde{C}_{nm}\left\{\delta(\omega)+\frac{1}{2}[\delta(\omega+2\Omega)+\delta(\Omega-2\Omega)]\right\} + \frac{\pi}{2}\frac{1}{\omega-E_{mm}+E_{nn}}[\delta(\omega+2\Omega)+\delta(\omega)] \times [\underline{\underline{\tilde{\chi}(\omega+\Omega)\tilde{V}}},\underline{\tilde{V}}]_{nm} + \frac{\pi}{2}\frac{1}{\omega-E_{mm}+E_{nn}} \times [\delta(\omega-2\Omega)+\delta(\omega)][\underline{\underline{\tilde{\chi}(\omega-\Omega)\tilde{V}}},\underline{\tilde{V}}]_{nm} \quad \text{(A12)}$$

and $[\underline{\underline{\tilde{\chi}(\omega)\tilde{V}}}]_{nm}$ has to be understood as $\tilde{\chi}_{nm}(\omega)\tilde{V}_{nm}$.

3. Third order

Finally, we evaluate the paramagnetic contribution to the third harmonic current $j^{x,(3)}_{para}$. Collecting all terms $\sim A_0^3$ in the equation of motion Eq. (10) results in the following equation for the third order correction to the density matrix:

$$i\dot{\underline{\underline{R}}}^{(3)}(t) = [\underline{\underline{R}}^{(3)}(t),\underline{\underline{H}}^{(0)}] + [\underline{\underline{R}}^{(2)}(t),\underline{\underline{V}}]f(t) + \tfrac{1}{2}[\underline{\underline{R}}^{(1)},\underline{\underline{C}}]f^2(t) - \tfrac{1}{6}[\underline{\underline{R}}^{(0)}(t),\underline{\underline{V}}]f^3(t). \quad \text{(A13)}$$

The solution for the contribution at $\omega = 3\Omega$ is then given by

$$\tilde{R}^3_{nm}(3\Omega) = -\frac{\pi}{24}\tilde{\chi}_{nm}(3\Omega)\tilde{V}_{nm} + \frac{\pi}{8}\frac{1}{3\Omega-E_{mm}+E_{nn}}[\underline{\underline{\tilde{\chi}(2\Omega)\tilde{C}}},\underline{\tilde{V}}]_{nm} + \frac{\pi}{8}\frac{1}{3\Omega-E_{mm}+E_{nn}}[\underline{\underline{\tilde{\chi}(\Omega)\tilde{V}}},\underline{\tilde{C}}]_{nm} + \frac{\pi}{4}\frac{1}{3\Omega-E_{mm}+E_{nn}} \times \left[\frac{1}{2\Omega-E_{mm}+E_{nn}}[\underline{\underline{\tilde{\chi}(2\Omega)\tilde{V}}},\underline{\tilde{V}}],\underline{\tilde{V}}\right]_{nm}. \quad \text{(A14)}$$

Not that in case of an isotropic s-wave SC with minimum energies $E_n = \pm\Delta$, Eq. (A14) has contributions at frequencies $3\Omega = 2\Delta$ and $2\Omega = 2\Delta$ in agreement with Ref. [21].

APPENDIX B: AVERAGING OVER FINITE SIZE EFFECTS

On finite lattices the SC gap is strongly influenced by the number of k points, in particular for d-wave systems where the gap vanishes along the nodal direction. This is shown in Fig. 6, where the minimum energy $E_{\min}$ is shown for a homogeneous $L \times L$ system and parameters used in the main paper, with L ranging from 40 to 80. As one can see, $E_{\min}$ reveals an "oscillatory" behavior as a function of L, due to the fact that the minimum gap depends on the "closeness" of a k point to the intersection of the underlying Fermi surface with the zone diagonal. In all cases the maximum spectral gap is $\approx 0.6t$. For a 60×60 lattice one finds a minimum SC gap of $\approx 0.08t$, while for a 68×68 lattice one has k points closer to the intersection between the Fermi surface and the zone diagonal, so that the minimum gap $E_{\min}$ is smaller ($\approx 0.004t$).

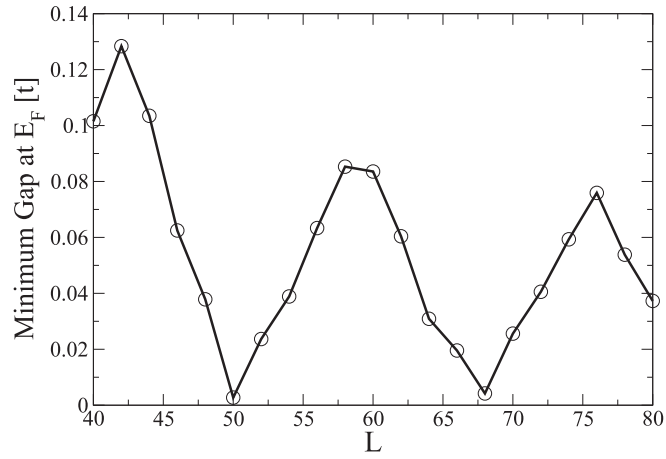

FIG. 6. Minimum SC gap in a homogeneous d-wave superconductor on a $L \times L$ lattice. $J/t = 1$, $n = 0.875$, and $t'/t = -0.2$.

Despite such an oscillatory behavior, for the lattice sites shown in Fig. 6 the set of k points which is sampled within such a period constitutes a mesh in momentum space dense enough to be representative of the behavior on a much larger lattice. This is demonstrated in Fig. 7. Here we show the comparison between the DOS of a large ($L = 800$) system and the DOS obtained as an average of the one computed over one period of oscillations for $E_{\min}$ in Fig. 6. More specifically, the average red curve is obtained by averaging the single DOS obtained for L ranging from 52 to 68, which are also shown for comparison in the inset. Here one sees that, while the individual densities still retain large oscillations for energies within the maximum SC gap, the averaged DOS is very close to the one obtained for the large $L = 800$ lattice, while some residual finite-size oscillations only survive for energies larger than the maximum gap. To minimize the effects of the finite lattice size we employed the same approach also for the computation of

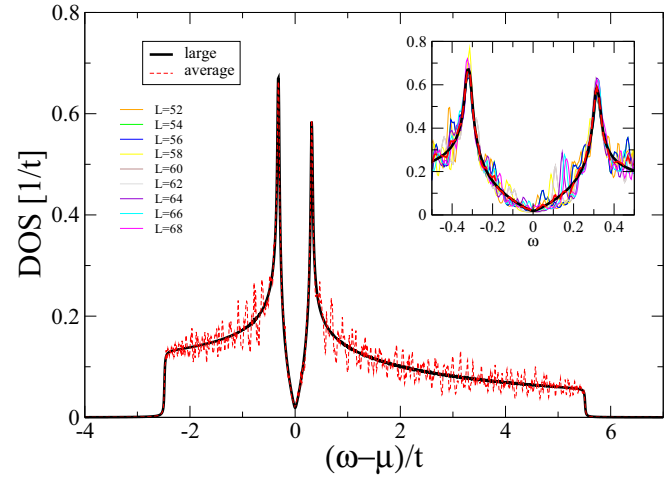

FIG. 7. Main panel: Density of states of a d-wave superconductor on a 800×800 lattice (black) compared to the average of spectral functions on $L \times L$ lattices with $52 \leqslant L \leqslant 68$ (red dashed). Inset: DOS from the individual finite lattices in the gap region. $J/t = 1$, $n = 0.875$, and $t'/t = -0.2$.

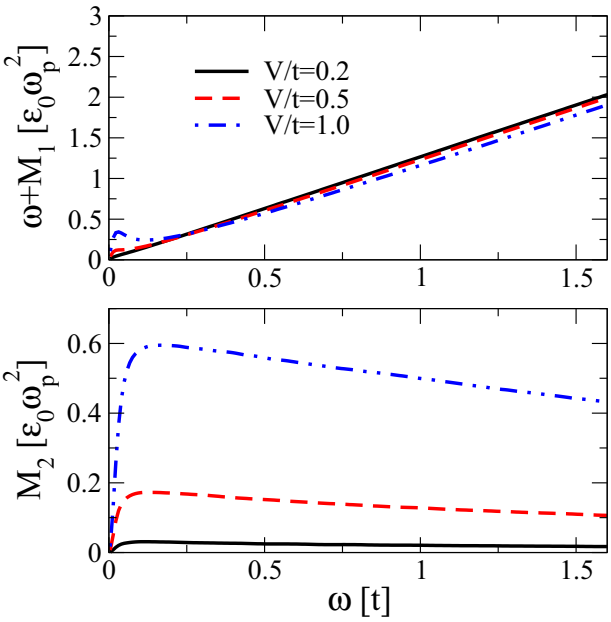

FIG. 8. Memory function for different disorder levels as extracted from the conductivities. $J/t = 1$, $n = 0.875$, and $t'/t = -0.2$.

the results in the inhomogeneous case, performing not only an average over disorder but also an average over different lattice sites.

APPENDIX C: UNIVERSAL CONDUCTIVITY OF *d*-WAVE SUPERCONDUCTORS

Within a Boltzmann-type approach, the dc conductivity of a disordered superconductor can be written as [53]

$$\sigma_{xx} = e^2 N_F v_F^2 \mathcal{T}_{xx}, \tag{C1}$$

where N_F is the normal-state DOS at the Fermi energy and $\mathcal{T}_{xx}$ plays the role of an effective transport time that is defined by the equation

$$\mathcal{T}_{xx} = \frac{\gamma^2}{v_F^2}\left\langle \frac{v_{F,x}^2(\phi)}{\sqrt{\Delta^2(\phi)+\gamma^2}^3}\right\rangle. \tag{C2}$$

Here $\langle \dots \rangle$ denotes the average over the Fermi surface, $v_F^2 \equiv \langle v_{F,x}^2(\phi)\rangle$, and γ is the width of the impurity band determined from

$$1 = \Gamma_{imp}\frac{\left\langle \frac{1}{\sqrt{\gamma^2+\Delta^2(\phi)}}\right\rangle}{C^2+\left\langle \frac{\gamma}{\sqrt{\gamma^2+\Delta^2(\phi)}}\right\rangle^2}. \tag{C3}$$

Γ_{imp} is proportional to the impurity concentration and C denotes the cotangent of the scattering phase shift. We solve Eqs. (C1) and (C2) for the homogeneous model Eq. (2) and parameters defined in Sec. II which yield a DOS of $N_F = 0.3051/t$. As a result we obtain $\sigma_0 = 2.38[e^2/\hbar]$ in the limit of vanishing disorder (equivalent to $C \to \infty$ and $\gamma \to 0$) and $\sigma_0 = 0.6[e^2/\hbar]$ in the strong-disorder unitary limit (equivalent to $C = 0$).

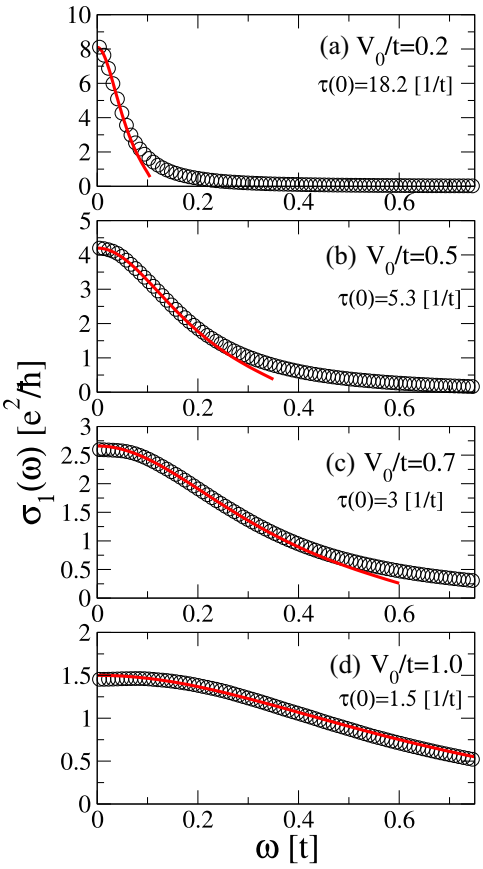

FIG. 9. Real part of the normal state conductivity (circles) at different disorder levels together with the fit from Eq. (D4) with the memory function Eq. (D5). $J/t = 1$, $n = 0.875$, and $t'/t = -0.2$.

APPENDIX D: DETERMINATION OF THE SCATTERING TIME IN THE NORMAL STATE

In order to extract the scattering time τ one could in principle fit the low-energy numerical normal state optical conductivity to the bare Drude form

$$\sigma(\omega) = \frac{\varepsilon_0 \omega_p^2}{-i\omega + \frac{1}{\tau}}, \tag{D1}$$

where ω_p denotes the plasma frequency. However, it is more convenient to start from a frequency-dependent optical conductivity represented in terms of a memory function $M(\omega)$ [61]

$$\sigma(\omega) = \frac{i\varepsilon_0 \omega_p^2}{\omega + M(\omega)}, \tag{D2}$$

which allows us to fit the numerical result over a larger frequency range and therefore yields a more robust value for τ.

Equation (D2) can be rewritten in a Drude-like form

$$\sigma(\omega) = \varepsilon_0 \omega_p^2 \frac{g(\omega)}{-i\omega + \frac{1}{\tau(\omega)}}, \tag{D3}$$

with

$$g(\omega) = \frac{1}{1 + \frac{M_1(\omega)}{\omega}}, \qquad \frac{1}{\tau(\omega)} = g(\omega) M_2(\omega),$$

so that the real part $\sigma_1(\omega)$ can be obtained from

$$\sigma_1(\omega) = \varepsilon_0 \omega_p^2 \frac{g(\omega)\tau(\omega)}{1 + \omega^2 \tau^2(\omega)}. \tag{D4}$$

Figure 8 shows the real M_1 and imaginary M_2 part of the memory function for three different disorder levels. We can approximately fit $M(\omega)$ with the formula

$$\omega + M(\omega) \approx A \ln \frac{B + \omega}{B - \omega} + iA\Theta(B - |\omega|). \tag{D5}$$

This approximation reproduces the linear behavior of $M_1(\omega) \sim \omega$ for small frequencies (approximately below $\omega/t \simeq 0.5$) and replaces the imaginary part $M_2(\omega)$ by a constant value above a threshold scale B. Such an approximation can be used to extrapolate M_2 at small frequencies in the regime where finite-size uncertainties set in. From Eq. (D5) the frequency-dependent scattering time reads

$$\tau(\omega) = \frac{1}{\omega} \ln \frac{B + \omega}{B - \omega}, \tag{D6}$$

with the zero frequency limit $\tau \equiv \tau(0) = 2/B$. Figure 9 shows that Eq. (D5) provides a good fit to the low-frequency conductivity. The corresponding zero-frequency scattering times derived from the above formula at each disorder level are reported in the panels.

We briefly comment on an alternative possibility, namely determining the scattering rate from the imaginary part $\sigma_2(\omega)$ in the normal state; cf. red dashed curves in the right panels of Fig. 1. From a conventional Drude picture one would expect

$$\omega\sigma_2(\omega) = \frac{\sigma_0}{\tau} \frac{\omega^2\tau^2}{1 + \omega^2\tau^2},$$

so that at $\omega\tau = 1$ the value of $\omega\sigma_2$ should be half the value at $\omega \to \infty$. Estimating the relaxation time from this approach yields slightly larger values than from the fitting of $\sigma_1(\omega)$ within the scheme outlined above, e.g., $\tau = 4/t$ instead of $\tau = 3/t$ for $V/t = 0.7$. In fact, fitting the memory function results in a more accurate description of the conductivity at low energies so that we consider these values of τ as more reliable.

[1] D. N. Basov, R. D. Averitt, D. van der Marel, M. Dressel, and K. Haule, Electrodynamics of correlated electron materials, Rev. Mod. Phys. **83**, 471 (2011).

[2] S. Tajima, Optical studies of high-temperature superconducting cuprates, Rep. Prog. Phys. **79**, 094001 (2016).

[3] C. Giannetti, M. Capone, D. Fausti, M. Fabrizio, F. Parmigiani, and D. Mihailovic, Ultrafast optical spectroscopy of strongly correlated materials and high-temperature superconductors: A non-equilibrium approach, Adv. Phys. **65**, 58 (2016).

[4] R. Shimano and N. Tsuji, Higgs mode in superconductors, Annu. Rev. Condens. Matter Phys. **11**, 103 (2020).

[5] R. Matsunaga, N. Tsuji, H. Fujita, A. Sugioka, K. Makise, Y. Uzawa, H. Terai, Z. Wang, H. Aoki, and R. Shimano, Light-induced collective pseudospin precession resonating with Higgs mode in a superconductor, Science **345**, 1145 (2014).

[6] R. Matsunaga, N. Tsuji, K. Makise, H. Terai, H. Aoki, and R. Shimano, Polarization-resolved terahertz third-harmonic generation in a single-crystal superconductor nbn: Dominance of the Higgs mode beyond the BCS approximation, Phys. Rev. B **96**, 020505(R) (2017).

[7] Z.-X. Wang, J.-R. Xue, H.-K. Shi, X.-Q. Jia, T. Lin, L.-Y. Shi, T. Dong, F. Wang, and N.-L. Wang, Transient Higgs oscillations and high-order nonlinear light-Higgs coupling in a terahertz wave driven NbN superconductor, Phys. Rev. B **105**, L100508 (2022).

[8] S. Kovalev, T. Dong, L.-Y. Shi, C. Reinhoffer, T.-Q. Xu, H.-Z. Wang, Y. Wang, Z.-Z. Gan, S. Germanskiy, J.-C. Deinert, I. Ilyakov, P. H. M. van Loosdrecht, D. Wu, N.-L. Wang, J. Demsar, and Z. Wang, Band-selective third-harmonic generation in superconducting MgB_2: Possible evidence for the Higgs amplitude mode in the dirty limit, Phys. Rev. B **104**, L140505 (2021).

[9] C. Reinhoffer, P. Pilch, A. Reinold, P. Derendorf, S. Kovalev, J.-C. Deinert, I. Ilyakov, A. Ponomaryov, M. Chen, T.-Q. Xu, Y. Wang, Z.-Z. Gan, D.-S. Wu, J.-L. Luo, S. Germanskiy, E. A. Mashkovich, P. H. M. van Loosdrecht, I. M. Eremin, and Z. Wang, High-order nonlinear terahertz probing of the two-band superconductor MgB_2: Third- and fifth-order harmonic generation, Phys. Rev. B **106**, 214514 (2022).

[10] K. Isoyama, N. Yoshikawa, K. Katsumi, J. Wong, N. Shikama, Y. Sakishita, F. Nabeshima, A. Maeda, and R. Shimano, Light-induced enhancement of superconductivity in iron-based superconductor $FeSe_{0.5}Te_{0.5}$, Commun. Phys. **4**, 160 (2021).

[11] H. Chu, M.-J. Kim, K. Katsumi, S. Kovalev, R. D. Dawson, L. Schwarz, N. Yoshikawa, G. Kim, D. Putzky, Z. Z. Li, H. Raffy, S. Germanskiy, J.-C. Deinert, N. Awari, I. Ilyakov, B. Green, M. Chen, M. Bawatna, G. Cristiani, G. Logvenov *et al.*, Phase-resolved Higgs response in superconducting cuprates, Nat. Commun. **11**, 1793 (2020).

[12] K. Katsumi, M. Nishida, S. Kaiser, S. Miyasaka, S. Tajima, and R. Shimano, Near-infrared light-induced superconducting-like state in underdoped $YBa_2Cu_3O_y$ studied by c-axis terahertz third-harmonic generation, Phys. Rev. B **107**, 214506 (2023).

[13] K. Kaj, K. A. Cremin, I. Hammock, J. Schalch, D. N. Basov, and R. D. Averitt, Terahertz third harmonic generation in c-axis $La_{1.85}Sr_{0.15}CuO_4$, Phys. Rev. B **107**, L140504 (2023).

[14] J. Y. Yuan, L. Y. Shi, L. Yue, B. H. Li, Z. X. Wang, S. X. Xu, T. Q. Xu, Y. Wang, Z. Z. Gan, F. C. Chen, Z. F. Lin, X. Wang, K. Jin, X. B. Wang, J. L. Luo, S. J. Zhang, Q. Wu, Q. M. Liu, T. C. Hu, R. S. Li *et al.*, Revealing strong coupling of collective modes between superconductivity and pseudogap in cuprate superconductor by terahertz third harmonic generation, arXiv:2211.06961.

[15] H. Chu, S. Kovalev, Z. X. Wang, L. Schwarz, T. Dong, L. Feng, R. Haenel, M.-J. Kim, P. Shabestari, L. P. Hoang, K.

Honasoge, R. D. Dawson, D. Putzky, G. Kim, M. Puviani, M. Chen, N. Awari, A. N. Ponomaryov, I. Ilyakov, M. Bluschke *et al.*, Fano interference between collective modes in cuprate high-Tc superconductors, Nat. Commun. **14**, 1343 (2023).

[16] M.-J. Kim, S. Kovalev, M. Udina, R. Haenel, G. Kim, M. Puviani, G. Cristiani, I. Ilyakov, T. V. A. G. de Oliveira, A. Ponomaryov, J.-C. Deinert, G. Logvenov, B. Keimer, D. Manske, L. Benfatto, and S. Kaiser, Tracing the dynamics of superconducting order via transient third harmonic generation, arXiv:2303.03288.

[17] N. Tsuji and H. Aoki, Theory of Anderson pseudospin resonance with Higgs mode in superconductors, Phys. Rev. B **92**, 064508 (2015).

[18] N. Tsuji, Y. Murakami, and H. Aoki, Nonlinear light-Higgs coupling in superconductors beyond BCS: Effects of the retarded phonon-mediated interaction, Phys. Rev. B **94**, 224519 (2016).

[19] T. Cea, C. Castellani, and L. Benfatto, Nonlinear optical effects and third-harmonic generation in superconductors: Cooper pairs versus Higgs mode contribution, Phys. Rev. B **93**, 180507(R) (2016).

[20] T. Cea, P. Barone, C. Castellani, and L. Benfatto, Polarization dependence of the third-harmonic generation in multiband superconductors, Phys. Rev. B **97**, 094516 (2018).

[21] M. Silaev, Nonlinear electromagnetic response and Higgs-mode excitation in BCS superconductors with impurities, Phys. Rev. B **99**, 224511 (2019).

[22] Y. Murotani and R. Shimano, Nonlinear optical response of collective modes in multiband superconductors assisted by nonmagnetic impurities, Phys. Rev. B **99**, 224510 (2019).

[23] N. Tsuji and Y. Nomura, Higgs-mode resonance in third harmonic generation in NbN superconductors: Multiband electron-phonon coupling, impurity scattering, and polarization-angle dependence, Phys. Rev. Res. **2**, 043029 (2020).

[24] L. Schwarz and D. Manske, Theory of driven Higgs oscillations and third-harmonic generation in unconventional superconductors, Phys. Rev. B **101**, 184519 (2020).

[25] G. Seibold, M. Udina, C. Castellani, and L. Benfatto, Third harmonic generation from collective modes in disordered superconductors, Phys. Rev. B **103**, 014512 (2021).

[26] M. A. Müller and I. M. Eremin, Signatures of bardasis-schrieffer mode excitation in third-harmonic generated currents, Phys. Rev. B **104**, 144508 (2021).

[27] J. Fiore, M. Udina, M. Marciani, G. Seibold, and L. Benfatto, Contribution of collective excitations to third harmonic generation in two-band superconductors: The case of MgB_2, Phys. Rev. B **106**, 094515 (2022).

[28] M. Udina, J. Fiore, T. Cea, C. Castellani, G. Seibold, and L. Benfatto, THz non-linear optical response in cuprates: Predominance of the BCS response over the Higgs mode, Faraday Discuss. **237**, 168 (2022).

[29] F. Gabriele, M. Udina, and L. Benfatto, Non-linear terahertz driving of plasma waves in layered cuprates, Nat. Commun. **12**, 752 (2021).

[30] K. Katsumi, Z. Z. Li, H. Raffy, Y. Gallais, and R. Shimano, Superconducting fluctuations probed by the Higgs mode in $Bi_2Sr_2CaCu_2O_{8+x}$ thin films, Phys. Rev. B **102**, 054510 (2020).

[31] F. Mahmood, X. He, I. Božović, and N. P. Armitage, Locating the missing superconducting electrons in the overdoped cuprates $La_{2-x}Sr_xCuO_4$, Phys. Rev. Lett. **122**, 027003 (2019).

[32] F. Mahmood, D. Ingram, X. He, J. A. Clayhold, I. Božović, and N. P. Armitage, Effect of radiation-induced defects on the superfluid density and optical conductivity of overdoped $La_{2-x}Sr_xCuO_4$, Phys. Rev. B **105**, 174501 (2022).

[33] I. Božović, X. He, J. Wu, and A. T. Bollinger, Dependence of the critical temperature in overdoped copper oxides on superfluid density, Nature (London) **536**, 309 (2016).

[34] N. R. Lee-Hone, V. Mishra, D. M. Broun, and P. J. Hirschfeld, Optical conductivity of overdoped cuprate superconductors: Application to $La_{2-x}Sr_xCuO_4$, Phys. Rev. B **98**, 054506 (2018).

[35] Z.-X. Li, S. A. Kivelson, and D.-H. Lee, Superconductor-to-metal transition in overdoped cuprates, npj Quantum Mater. **6**, 36 (2021).

[36] M. Pal, A. Kreisel, W. A. Atkinson, and P. J. Hirschfeld, Simulating superconducting properties of overdoped cuprates: The role of inhomogeneity, Phys. Rev. B **107**, 144501 (2023).

[37] P. A. Lee, Localized states in a d-wave superconductor, Phys. Rev. Lett. **71**, 1887 (1993).

[38] A. C. Durst and P. A. Lee, Impurity-induced quasiparticle transport and universal-limit Wiedemann-Franz violation in d-wave superconductors, Phys. Rev. B **62**, 1270 (2000).

[39] A. Ghosal, M. Randeria, and N. Trivedi, Spatial inhomogeneities in disordered d-wave superconductors, Phys. Rev. B **63**, 020505(R) (2000).

[40] D. Chakraborty, R. Sensarma, and A. Ghosal, Effects of strong disorder in strongly correlated superconductors, Phys. Rev. B **95**, 014516 (2017).

[41] D. Chakraborty, N. Kaushal, and A. Ghosal, Pairing theory for strongly correlated d-wave superconductors, Phys. Rev. B **96**, 134518 (2017).

[42] A. Ghosal, M. Randeria, and N. Trivedi, Inhomogeneous pairing in highly disordered s-wave superconductors, Phys. Rev. B **65**, 014501 (2001).

[43] K. Bouadim, Y. L. Loh, M. Randeria, and N. Trivedi, Single- and two-particle energy gaps across the disorder-driven superconductor–insulator transition, Nat. Phys. **7**, 884 (2011).

[44] G. Seibold, L. Benfatto, C. Castellani, and J. Lorenzana, Superfluid density and phase relaxation in superconductors with strong disorder, Phys. Rev. Lett. **108**, 207004 (2012).

[45] G. Lemarié, A. Kamlapure, D. Bucheli, L. Benfatto, J. Lorenzana, G. Seibold, S. C. Ganguli, P. Raychaudhuri, and C. Castellani, Universal scaling of the order-parameter distribution in strongly disordered superconductors, Phys. Rev. B **87**, 184509 (2013).

[46] A. Samanta, A. Ratnakar, N. Trivedi, and R. Sensarma, Two-particle spectral function for disordered s-wave superconductors: Local maps and collective modes, Phys. Rev. B **101**, 024507 (2020).

[47] B. Fan, A. Samanta, and A. M. García-García, Characterization of collective excitations in weakly coupled disordered superconductors, Phys. Rev. B **105**, 094515 (2022).

[48] C. N. Breiø, P. J. Hirschfeld, and B. M. Andersen, Supercurrents and spontaneous time-reversal symmetry breaking by nonmagnetic disorder in unconventional superconductors, Phys. Rev. B **105**, 014504 (2022).

[49] I. Hashimoto, M. Vishik, R. He, T. P. Devereaux, and Z. Shen, Energy gaps in high-transition-temperature cuprate superconductors, Nat. Phys. **10**, 483 (2014).

[50] R. S. Markiewicz, S. Sahrakorpi, M. Lindroos, H. Lin, and A. Bansil, One-band tight-binding model parametrization of the

high-T_c cuprates including the effect of k_z dispersion, Phys. Rev. B **72**, 054519 (2005).

[51] J. P. Blaizot and G. Ripka, *Quantum Theory of Finite Systems* (MIT Press, Cambridge, MA, 1986).

[52] G. Seibold, L. Benfatto, and C. Castellani, Application of the mattis-bardeen theory in strongly disordered superconductors, Phys. Rev. B **96**, 144507 (2017).

[53] M. J. Graf, S.-K. Yip, J. A. Sauls, and D. Rainer, Electronic thermal conductivity and the Wiedemann-Franz law for unconventional superconductors, Phys. Rev. B **53**, 15147 (1996).

[54] W. A. Atkinson and P. J. Hirschfeld, Optical and thermal-transport properties of an inhomogeneous d-wave superconductor, Phys. Rev. Lett. **88**, 187003 (2002).

[55] J. Corson, J. Orenstein, S. Oh, J. O'Donnell, and J. N. Eckstein, Nodal quasiparticle lifetime in the superconducting state of $Bi_2Sr_2CaCu_2O_{8+\delta}$, Phys. Rev. Lett. **85**, 2569 (2000).

[56] H. Won and K. Maki, d-wave superconductor as a model of high-T_c superconductors, Phys. Rev. B **49**, 1397 (1994).

[57] L. Zhu, P. J. Hirschfeld, and D. J. Scalapino, Elastic forward scattering in the cuprate superconducting state, Phys. Rev. B **70**, 214503 (2004).

[58] J. Schrieffer, *Theory of Superconductivity*, Frontiers in Physics (Addison-Wesley, Redwood City, CA, 1988).

[59] K. Katsumi, N. Tsuji, Y. I. Hamada, R. Matsunaga, J. Schneeloch, R. D. Zhong, G. D. Gu, H. Aoki, Y. Gallais, and R. Shimano, Higgs mode in the d-wave superconductor $Bi_2Sr_2CaCu_2O_{8+x}$ driven by an intense terahertz pulse, Phys. Rev. Lett. **120**, 117001 (2018).

[60] L. Feng, J. Cao, T. Priessnitz, Y. Dai, T. de Oliveira, J. Yuan, R. Oka, M.-J. Kim, M. Chen, A. N. Ponomaryov, I. Ilyakov, H. Zhang, Y. Lv, V. Mazzotti, G. Kim, G. Christiani, G. Logvenov, D. Wu, Y. Huang, J.-C. Deinert, S. Kovalev *et al.*, Dynamical interplay between superconductivity and charge density wave: A nonlinear terahertz study of coherently driven 2H-$NbSe_2$, Phys. Rev. B **108**, L100504 (2023).

[61] W. Götze and P. Wölfle, Homogeneous dynamical conductivity of simple metals, Phys. Rev. B **6**, 1226 (1972).